Applied Catalysis B: Environmental 180 (2016) 351–361

Contents lists available at ScienceDirect

Applied Catalysis B: Environmental

journal homepage: www.elsevier.com/locate/apcatb

Influence of synthesis method on leaching of the Cr-TiO_2 catalyst for visible light liquid phase photocatalysis and their stability

Siva Nagi Reddy Inturi[a], Makram Suidan[b,**], Panagiotis G. Smirniotis[a,*]

[a] Chemical Engineering Program, Department of Biomedical, Chemical, and Environmental Engineering, University of Cincinnati, Cincinnati, OH 45221-0012, USA

[b] Engineering College and Architecture, American University of Beirut, Beirut 1107-2020, Lebanon

ARTICLE INFO

Article history:
Received 31 October 2014
Received in revised form 17 May 2015
Accepted 22 May 2015
Available online 27 June 2015

Keywords:
Flame spray pyrolysis (FSP)
Titania
TiO_2
Visible-light-induced
Liquid phase
Photodegradation
Leaching
Secondary metal contamination

ABSTRACT

Cr-TiO_2 nanoparticles have been synthesized by using flame spray pyrolysis (FSP), co-precipitation, and sol–gel synthesis techniques. Liquid phase photocatalytic activity of the synthesized catalysts by various methods were studied for photocatalytic degradation of 4-chlorophenol under visible light (400–800 nm) conditions. It was found that the FSP Cr-TiO_2 has superior photocatalytic activity to other synthesis methods. XRD patterns showed that the anatase phase was higher for the sol–gel and co-precipitation made catalyst. Our TPR results indicated higher presence of the Cr^{+6} of the FSP made catalysts in comparison to the other ones, which had significant influence in the activity of the catalyst. All the three catalysts showed the decline in the activity which was a consequence of the decrease of Cr^{+6} content of the catalyst along with the forming agglomerates in the spent and reactivated catalyst. The leaching of the Cr into the liquid phase for pH ranging from 3 to 11 was studied of the FSP made catalyst and was found to be minimal with respect to other synthesis methods. For this reason there should be careful consideration for use of Cr containing catalysts for practical water treatment. We developed Si/Ti/Cr catalyst by FSP method which stabilizes the photocatalytic activity of the catalyst. The BET surface area of the FSP Si/Ti/Cr catalyst was stable even with the reactivated catalyst. The developed catalyst also demonstrated an advantage of low levels of metal leaching during the catalytic reaction thus avoiding secondary metal contamination to the treated wastewater. We found higher Cr(VI) concentration in the reactivated materials which is a significant factor for the improvement in the photocatalytic activity of the materials. We have observed the improvement in the activity with the addition of Si by FSP method as a support and it also caused the improvement in the surface area and structural stability.

Published by Elsevier B.V.

1. Introduction

Photocatalysis has gained a substantial amount of attention due to its potential environmental applications towards water treatment, such as purifying polluted air and waste water streams, self-cleaning materials and the creation of new chemicals [1–3]. There has been a major attention towards the visible light photocatalysis of waste water due to its flexibility and cost-effective breakdown of harmful organic molecules at ambient conditions. During the photocatalytic process, when the light (photons) with sufficient energy is absorbed on the catalyst leads to the excitation of electrons from the valence band to the conduction band, thus generating electron–hole pairs. The photo-generated holes will form hydroxyl radicals when they react with the OH^-/water over the surface of the catalyst. The degradation of the organic compounds in the air/water stream is caused due to these highly active radicals [4–5].

Among the semiconductors known, TiO_2 is widely used as catalyst for the environmental applications due to its resistance to corrosion, non-toxicity, physical and chemical stability and low cost. In order to succeed, it is essential to utilize the light source of satisfactory intensity so as to acquire energy that exceeds the TiO_2 band gap energy (E_{bg}). However, the large band gap of the TiO_2 (E_{bg}(anatase) = 3.2 eV), requires a wavelength of 400 nm or less for the excitation of the catalyst [5]. The incorporation of transition metal/metal oxides in the TiO_2 crystal lattice may result in the formation of new energy levels between the valence band and the conduction band, thus inducing a shift of light absorption towards the visible light region. The photocatalytic activity usually depends on the nature and the amount of doping agent. The

* Corresponding author. Fax: +1 513 556 3473.
** Corresponding author.
E-mail addresses: makram.suidan@uc.edu, msuidan@aub.edu.lb (M. Suidan), panagiotis.smirniotis@uc.edu (P.G. Smirniotis).

http://dx.doi.org/10.1016/j.apcatb.2015.05.046
0926-3373/Published by Elsevier B.V.

use of supported titanium dioxide has allowed enhancing the photodegradation rates in comparison with pure TiO_2 [6–10]. Doping TiO_2 with metal ions can enhance its photoactivity [11] or even can enable its sensitization under visible light [12].

In earlier studies involving transition metal doped TiO_2 [11–14], it was shown that among all the transition doped metals Cr had higher photocatalytic activity under visible light [11–15]. The activity of the catalyst depends on the amount of Cr(IV) in the catalyst and the mechanism in these systems was the creation of the electron and hole pair by the additional effect of reduction by the electrons of the TiO_2 conduction band of Cr(IV) to Cr(V) and regeneration of Cr(IV) from Cr(V) [16,18]. The photocatalytic activity of Cr/TiO_2 for the degradation of the organic pollutants in visible light attracts significant interest for future environmental applications. However, the Cr/TiO_2 systems as photocatalysts have some challenges such as the leaching of the Cr in the liquid stream. In addition, Cr(VI) may undergo a subsequent reduction to Cr(III). There is not much literature available to study the secondary contamination caused by the metal leaching due to the catalyst and its effect due to the synthesis methods. Most of these research works commonly encountered with a problem that the efficiency of the catalyst deteriorated rapidly [15–18]. This fact rendered the photocatalytic oxidative system unfeasible for treating waste water streams continuously. To overcome this shortcoming, we need to understand the effect of different synthesis methods for their stability at a wide range of pH (3–11). Many synthesis methods of anatase TiO_2 have been conducted by researchers such as inert gas condensation, sol–gel, solvo thermal, flame synthesis by oxidation, oxidation–hydrothermal and hydrolysis precipitation of titanium alkoxides or inorganic salts [19–25]. We know that the structural and surface properties of the materials are influenced by the synthesis methods employed.

The present study mainly aimed at investigating the influence of synthesis method on the liquid phase photocatalytic activity of 4-chlorophenol under visible light (400–800 nm). We intended on developing a catalyst with high photocatalytic activity as well as superior stability. For this purpose, we synthesized Cr/TiO_2 by using three different methods, namely; co-precipitation, sol–gel, and flame spray pyrolysis synthesis methods [26–27]. For comparison purpose, we also synthesized pure TiO_2 by the flame spray pyrolysis method. We have used the catalyst for five runs to observe the stability. Among the various catalysts, Cr/TiO_2 synthesized by FSP method exhibits higher photocatalytic activity but ineffective to attain stability. To enhance the stability of the catalyst, 1:1:0.4 Si/Ti/Cr was synthesized. The fresh and spent catalysts were characterized by various techniques to understand the effect of properties on synthesis method and addition of Si. 4-Chlorophenol is chosen as the model organic compound for the photocatalytic oxidation studies. It is frequently observed in various civil and industrial waste waters. 4-Chlorophenol is also detected as an in-door air component emitted by commercial fibrous polymeric materials, resins and smoking tobacco.

2. Experimental

2.1. Catalyst synthesis

2.1.1. Co-precipitation

Both TiO_2 and Cr were precipitated together by using Ammonium hydroxide as a precipitating agent. In this preparation, 12 g of titanium-tetra-isopropoxide (TTIP, Sigma–Aldrich, purity N97%) was dissolved in nitric acid solution (2 M) and chromium nitrate were dissolved separately in deionized water. The atomic ratio of Ti/Cr was kept at 40. The aqueous solutions were mixed thoroughly. Aqueous Ammonium hydroxide was added gradually drop wise to the mixture solutions, and vigorously stirred; until precipitation was complete (pH 11). The obtained precipitate gels were further aged overnight, and filtered off. The obtained filtered precipitate was dried in oven at 80 °C for 12 h. Finally, the catalyst was calcined at 500 °C for 5 h in the presence of air with 5 °C/min ramping.

2.1.2. Sol–gel method

Cr/TiO_2 nanoparticles were prepared by standard so–gel methods. TiO_2 sols were prepared by drop wise addition of 5 mL of an ethanolic TTIP solution, which had been dissolved in 50 mL of absolute ethanol, into 50 mL of distilled water adjusted to pH 1.5 with nitric acid under vigorous stirring at room temperature. $Cr(NO_3)_3{\cdot}9H_2O$ (Adrich) was added to the TiO_2 sol. After continuously stirring for 24 h, the resulting transparent solution was evaporated using a rotary evaporator at 45 °C and dried in the oven (70 °C) overnight. The obtained powder was calcined at 500 °C for 5 h under air.

2.1.3. Flame spray pyrolysis (FSP) method

The synthesis procedure for the flame-made nanoparticles is explained in detail in our previous studies [28–30]. Briefly, a mixture of *o*-xylene (Sigma–Aldrich Reagent, 99%) /acetonitrile (Sigma–Aldrich Reagent) in the volume ratio of 3/1 was used as the solvent. For pure FSP made TTIP was used as a precursor and diluted with the solvent to a 0.3 M solution metal oxide nanoparticles were synthesized by a one-step FSP synthesis technique. Precursor solutions resulting in powders of chromium incorporated TiO_2 were prepared by dissolving predetermined amounts of TTIP and chromium precursor (Chromium(III) 2-ethylhexanoate, Strem, 70% in mineral spirits Cr). The total molar metal (Ti + Cr and Ti + Si + Cr) concentration of in the liquid precursor was set at 0.3 M. For Si/Ti/Cr synthesis tetraethyl-orthosilicate (TEOS, Sigma–Aldrich, purity N98%) as the Si source was used. The ratio of Si/Ti is kept at 1 and M(Si + Ti)/Cr ratio of 20. During FSP, the liquid precursor was fed through a spray nozzle at a flow rate of 3 mL min^{-1} using a syringe pump (Cole Parmer, 74900 series), where it was dispersed by a surrounding 5 L min^{-1} flow of O_2 (1.5 bar, Wright Brothers, 99.98%). Combustion of the dispersed droplets was ignited by a surrounding supporting flame (premixed 1.0 L min^{-1} O_2/1.0 L min^{-1} CH_4). Additionally, 3 L/min sheath O_2 (BOC Gases) was issued through the outermost sintered metal ring. Fine aerosol nanoparticles leaving the flame were collected on a flat glass fiber filter (Whatman GF/A, 150 mm in diameter) aided by a vacuum pump (Grainger Inc.) [17–18]. The aerosol nanoparticles were scraped from the filter for direct use as catalyst without any further treatment. The metal components of the catalysts are denoted Ti/Cr.

2.2. Characterization

2.2.1. BET measurements

The BET specific surface area of the as-prepared nanoparticles was determined from nitrogen adsorption equilibrium isotherm sat liquid nitrogen temperature (77 K) using an automated gas sorption system (Micromeretics ASAP 2010) operating in continuous mode. Prior to the analysis, 0.050 ± 0.005 g of catalyst was evacuated under a helium atmosphere for 3 h at 250 °C in the degaussing part of the instrument. The adsorption isotherms of nitrogen were collected at 77 K using approximately six values and by taking 0.162 nm^2 as the molecular area of the nitrogen molecule. Specific surface areas of the samples were determined by nitrogen adsorption data in the relative pressure range from 0.05 to 0.3 using the Brunauer–Emmett–Teller (BET) equation. Total pore volumes were determined from the amount of gas adsorbed at the relative pressure of 0.99.

2.2.2. X-ray diffraction

The Powder X-ray diffraction (XRD) patterns were employed for the identification of phases of the synthesized metal oxide nanoparticles. The XRD patterns were recorded on a Phillips Xpert diffractometer using nickel–filtered CuKα (wavelength 0.154056 nm) radiation source and a scintillation counter detector. An aluminium holder was used to support the catalyst samples. The intensity data were collected over a 2θ range of 10°–80° with a step size of 0.025° and a step time of 0.50 s. Crystalline phases were identified by comparison with the reference data from the International Center for Diffraction Data (ICDD) files.

2.2.3. UV–vis spectroscopy

The catalyst powders were characterized by UV–vis spectrophotometer (Shimadzu 2501PC) with an ISR1200 integrating sphere attachment for their diffuse reflectance with the wavelength ranging from 200 to 900 nm. $BaSO_4$ was used as the standard for these measurements.

2.2.4. Transmission electron microscopy (TEM)

Selected fresh catalyst samples were characterized with a Philips CM 20 electron microscope. The samples were sonically dispersed in isopropyl alcohol and transferred into carbon-Cu grid and after complete evaporation of the isopropyl alcohol, the particles attached to the walls of the holes in the carbon film were examined. The applied accelerating voltage was 200 keV, with a LaB_6 emission current and a point-to-point resolution of 0.27 nm.

2.2.5. Temperature programmed reduction (H_2–TPR)

H_2–TPR of as-prepared aerosol nanoparticles was performed using an automated catalyst characterization system (Micromeritics model AutoChem2910). Prior to the analysis approximately 0.050 g of the catalysts were pretreated at 250 °C for 2 h in ultrahigh pure helium (30 mL min^{-1}) stream. A mixture of isopropanol and liquid nitrogen was used in the trapper to collect the formed water during the TPR experiment. After preheating, samples were tested by increasing the temperature from 50 to 800 °C. The temperature was then kept constant at 800 °C until the signal of hydrogen consumption returned to the initial values. The temperature programmed reduction runs were carried out with a linear heating rate (10 °C/min) in a flow of 10% H_2 in Argon with a flow rate of 20 mL min^{-1}. The hydrogen consumption was measured quantitatively by a thermal conductivity detector.

2.2.6. ICP-MS leaching of metal study

100 mL of water containing 100 mg of the catalyst was taken in 250 mL beaker. pH (3, 5, 7, 9 and 11) were obtained by adding diluted HCl and NaOH dropwise. After reaching the anticipated pH, the solution was stirred for 24 h. Then, the solution was filtered and labelled. ICPMS-based quantification has been commonly used to determine accurate trace concentration of multiple metals simultaneously in samples. The metal ion analysis and speciation was carried out by using state-of-the-art inductively coupled plasma-mass spectrometry (ICP-MS) Agilent 8800 ICP-QQQ. A conventional Meinhard nebulizer, a Peltier-cooled spray chamber (2 °C) and a shield torch constitute the sample introduction system under standard plasma conditions. The metal concentration on the catalyst was measured by an inductively coupled plasma (ICP) atomic emission spectrometer.

2.3. Photocatalysis

The catalysts prepared were tested with the photo-degradation of 4-chlorophenol, which was performed in a batch round, flat-plate reactor described elsewhere [31]. A double acrylic OP-2 (Museum quality) sheet was placed between the light source and the reactor for the purpose of excluding ultraviolet radiation when conducting visible-light experiments [18]. The reactor is surrounded by with six F8T5 ww lamps. The cooling jacket around the reactor allowed to effectively preclude the IR part of the spectrum from penetrating into the reaction solution and cooled the lamp. The temperature of the reaction was kept at 25 °C. 400 mg of catalyst was mixed with 500 mL of 500 μm 4-chlorophenol. The pH of the reaction suspension was not adjusted. The suspended catalyst in aqueous system was oxygenated (Wright Brothers, 99.9%) at 0.5 L/min to assure the complete saturation. The samples of reaction suspension were collected with a syringe at different intervals and filtered with Cameo 25 P polypropylene syringe filters (OSMONICS, Cat# DDP02T2550). The sample solutions were analyzed with a total organic carbon analyzer (TOC-VCSH, Shimadzu).

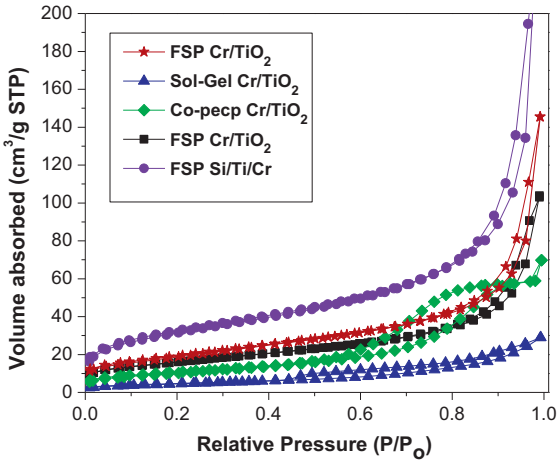

Fig. 1. Nitrogen adsorption and desorption isotherms of Cr/TiO_2 catalysts made by FSP, sol–gel and co-precipitation.

2.3.1. Regeneration of the deactivated photocatalyst

The used catalysts were found to be reduced during the photoreactions, which resulted in deactivation of the catalysts. The suspensions of the catalyst particles after each reaction experiment were filtered with a cellulose nitrate membrane filter (0.2 mm in pore size, MFS, A020A090C). The obtained deactivated catalyst was reactivated by the calcination of the used catalyst at 450 °C under air flow for 3 h. Afterwards, the reactivated catalysts were characterized with a UV–vis spectrometer. The pore size and pore volume of the reactivated catalyst were measured on the Micromeritics 2010 analyzer. The photoactivity of the reactivated catalyst by calcinations was studied under visible light with the same setup that was used in the previous experiment. The prefix RA was used for the reactivated catalyst followed by the showing the number of reactivation cycles. The prefix R represented the catalysts which are reused without activation.

3. Results and discussion

3.1. BET surface area, pore size and pore volume

Fig. 1 shows the nitrogen adsorption and desorption isotherms at 77 K which provides the indications of the presence of the pore size and structure. The nitrogen adsorption–desorption isotherms of TiO_2/Cr synthesized by different methods and TiO_2 sample exhibits type IV sorption isotherms with a type H3 hysteresis loop according to UPAC classification [32], which indicates the existence of mesopores in the corresponding materials. These catalysts showed an adsorption–desorption hysteresis cycle, which can be attributed to capillary condensation in mesoporous solids. It is

Table 1
BET characterization results for the materials.

Catalyst	Isotherm type[a]	SSA (m^2/g)	d_{BET}[b] (nm)	Pore volume (cm^3/g)	Pore diameter(nm)
FSP TiO_2	IV	51	30	0.18	15
FSP Cr/TiO_2	IV	93	16	0.3	16
R1 FSP Cr/TiO_2	IV	59	25	0.30	23
RA1 FSP Cr/TiO_2	IV	54	28	0.41	3
R5 FSP Cr/TiO_2	IV	49	30	0.29	7
RA5 FSP Cr/TiO_2	IV	41	36	0.5	3
Sol–gel Cr/TiO_2	IV	29.1	54	0.04	10
R1 sol–gel Cr/TiO_2	IV	27.2	57	0.05	9
RA1 sol–gel Cr/TiO_2	IV	26.3	59	0.04	9
Co-preci. Cr/TiO_2	IV	56.9	27	0.1	10
R1Co-preci. Cr/TiO_2	IV	51.1	30	0.1	9
RA1Co-preci. Cr/TiO_2	IV	49	32	0.1	8
FSP Si/Ti/Cr	III	140	11	0.35	15
R1 FSP Si/Ti/Cr	III	139	11	0.52	17
RA1 FSP Si/Ti/Cr	III	137	11	0.5	17
R3 FSP Si/Ti/Cr	III	131	11	0.48	18
RA3 FSP Si/Ti/Cr	III	126	12	0.38	19

[a] Isotherm type is based on IUPAC nomenclature.
[b] d_{BET} is average unit cell parameter calculated based on mass weight average density of anatase and rutile phases determined by XRD.

believed that this type of loop, exhibiting no limiting adsorption at high P/P_0, results from the assembly of loosely coherent particles. One can observe that the catalyst undergoes a monotonical increase in the adsorbed volume at a high relative pressure followed by a plateau, which is in turn a characteristic of solid microporous. The type H4 loop is associated with narrow slit-like pores. Some other researchers also observed similar adsorption and desorption isotherms for the nanoporous materials [33–34]. Table 1 shows the BET surface area of the photocatalysts used in this study. The BET surface area of pure Cr/TiO_2 (93 m^2/g) is much higher than Cr/TiO_2 synthesized by sol–gel (29.1 m^2/g) and co-precp (57 m^2/g). We have observed higher surface area of the catalyst synthesized by FSP method TiO_2 (109 m^2/g), Cr/TiO_2 (93 m^2/g) and Si/Ti/Cr (140 m^2/g). We have observed negligible change in the surface area of the Si/Ti/Cr catalyst for the fresh, used and reactivated catalysts. The observed reduction in the BET surface area of the Cr/TiO_2 may possibly be due to the formation of agglomerates of the catalyst and the collapse of the structure of the catalyst. A stable, high surface area with a three-dimensional mesoporous structure can achieve much facile adsorption/desorption equilibrium and mass diffusion of reactants and products and thus enhance the activity and stability of the Si/Ti/Cr materials in the photocatalytic application.

3.2. XRD characterization

Fig. 2(a) and (b) shows the wide angle powder X-ray diffraction patterns for the catalyst synthesized by different methods (co-precipitation, sol–gel and FSP). The diffractogram patterns of pure TiO_2 synthesized by FSP also presented for the comparison purpose. For the FSP TiO_2, the strong characteristic peaks of titania observed (typically at d = 3.54, 1.90, and 2.40 Å, which correspond to anatase phase (JCPDS #21-1272)). In order to ensure the effects of Cr doping by the different synthesis methods on the anatase-rutile phase transformation, the fraction of rutile, X_R was calculated from the respective peak intensities using the following equation:

$$X_R\% = \left(1 - \frac{1}{1 + \frac{1.26 \times I_R}{I_A}}\right) \times 100 \quad (1)$$

where, I_R and I_A are the X-ray intensities of the rutile (1 1 0) and anatase (1 0 1) peaks, respectively. These relative rutile and anatase fractions are listed in Table 2. The rutile fractions of fresh FSP Cr/TiO_2 was estimated from Eq. (1) to be 34%. We can observe that there is no rutile phase present for the catalyst prepared by sol–gel and co-precp methods. We can see in Fig 2(a) the fraction of the anatase phase for the R1 and RA1 of the catalyst synthesized by both

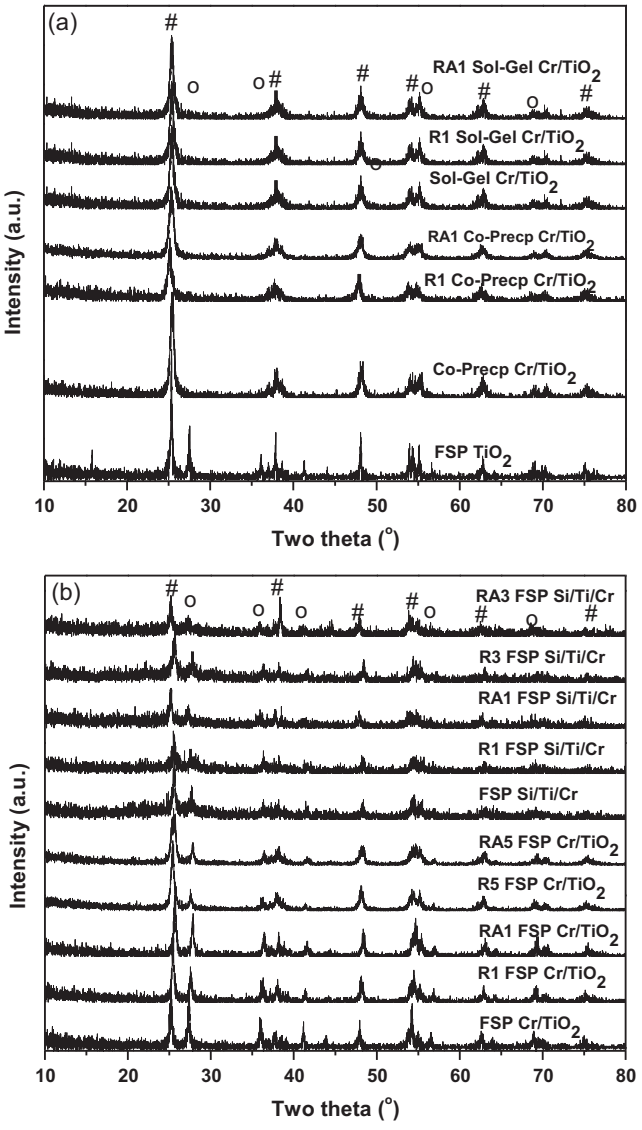

Fig. 2. Powder X-ray diffraction patterns of fresh, used reactivated catalysts made by (a) FSP TiO_2, sol–gel and co-precipitation; (b) FSP TiO_2, FSP Cr/TiO_2, FSP Si/Ti/Cr (with atomic ratio of 20:20:2); (# → anatase TiO_2 and O → rutile TiO_2).

Table 2
XRD and UV–vis spectroscopy characterization results for our catalyst.

Catalyst	$X_{Anatase}$ [a],(%)	d_A [b],(nm)	d_R [b],(nm)	D_{XRD} [c],(nm)	Band gap, (eV)
FSP TiO_2	81	28	125	47	3.17
FSP Cr/TiO_2	66	148	222	174	2.61
R1 FSP Cr/TiO_2	60	53	185	106	2.22
RA1 FSP Cr/TiO_2	56	53	278	153	2.21
R5 FSP Cr/TiO_2	54	46	230	130	2.14
RA5 FSP Cr/TiO_2	57	42	208	113	2.11
Sol–gel Cr/TiO_2	100	74	0	74	1.96
R1 sol–gel Cr/TiO_2	100	37	0	37	1.90
RA1 sol–gel Cr/TiO_2	100	32	0	32	1.86
Co-preci. Cr/TiO_2	100	41	0	41	1.73
R1Co-preci. Cr/TiO_2	93	37	79	40	2.00
RA1Co-preci. Cr/TiO_2	99	36	77	36	2.08
FSP Si/Ti/Cr	70	93	93	93	2.22
R1 FSP Si/Ti/Cr	69	53	69	58	2.14
RA1 FSP Si/Ti/Cr	68	62	185	102	2.18
R3 FSP Si/Ti/Cr	67	93	185	124	2.18
RA3 FSP Si/Ti/Cr	77	93	93	93	2.18

[a] $X_{anatase}$ (%) = 100 − X_{rutile} (%).
[b] d_A and d_R are the crystallite sizes of anatase and rutile, respectively.
[c] D_{XRD} is the mass weighted average crystal diameter using the Scherrer equation.

sol–gel and co-precp methods. This could be due to the calcination step involved in the synthesis process which has enhanced the formation of anatase phase. The intensities of the anatase peak for the catalyst synthesized by sol–gel and co-precp. methods has found to be higher than the FSP made materials which indicates the presence of more crystalline phase for the former materials. The RA1 of the catalyst by sol–gel and co-precp has showed more intensity than the R1 which is a result of secondary calcination of the used catalyst. No characteristic peaks of chromium oxides (Cr_2O_3 and CrO_2) were found in the XRD patterns. These results suggest that the doping levels we employed did not induce the formation of discrete impurity phases and that the metal ion appears to have been integrated into the basic structure of TiO_2. However, it is conceivable that chromium oxides, which were formed during synthesis dispersed over the surface. Thus, the crystal structure of TiO_2 indicates a mixture of anatase and rutile for all the as-synthesized Cr/TiO_2 samples.

The X-ray powder diffraction patterns are also used to determine the crystallite size of all the prepared samples. The crystallite size τ is determined from the broadening of the peaks by Scherrer's formula [35].

$$\tau = \frac{K\lambda}{\beta_\tau \cos\theta} \quad (2)$$

where, K the shape factor = 0.9; β_τ is the width of the peak at half the maximum intensity (FWHM) after subtraction of instrumental noise and 2θ is the diffraction angle. The estimation shows that the mean crystal size of the initial anatase TiO_2 individual particles calculated from Eq. (2) was 32–148 nm. The N_2 physi-adsorption measured the primary particle size from the surface area of the catalyst smaller then the crystal size calculated from XRD.This could be explained by the bimodal particle-size distributions observed for flames with low enthalpy content and precursors of low thermal stability. FSP materials synthesis from liquid precursor could result in bimodal particle size distributions because of the insufficient evaporation energy and temperature [36].

X-ray diffraction pattern of TiO_2 and chromium doped TiO_2 nanoparticles are shown in Fig. 2(a) and (b). Each diffraction pattern corresponds to the mixed (anatase + rutile) phases of TiO_2. A close inspection of the intense (1 0 1) peak reveals that doping of chromium shifts the diffraction peaks slightly to higher angle. In octahedral coordination, the ionic radii of different valence states of chromium are Cr^{3+} (0.75 Å), Cr^{4+} (0.69 Å), Cr^{5+} (0.63 Å), Cr^{6+} (0.58 Å), respectively [37]. The anatase content for the FSP Si/Ti/Cr

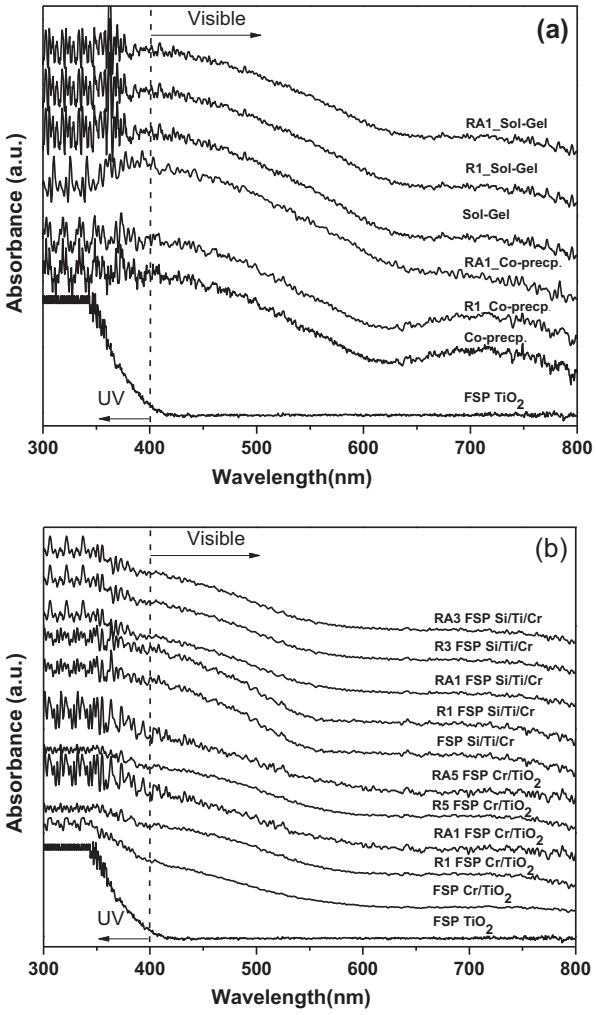

Fig. 3. UV–vis diffuse reflectance spectra of fresh, used reactivated catalysts made by (a) FSP TiO_2, sol–gel and co-precipitation; (b) FSP TiO_2, FSP Cr/TiO_2, FSP Si/Ti/Cr (with atomic ratio of 20:20:2).

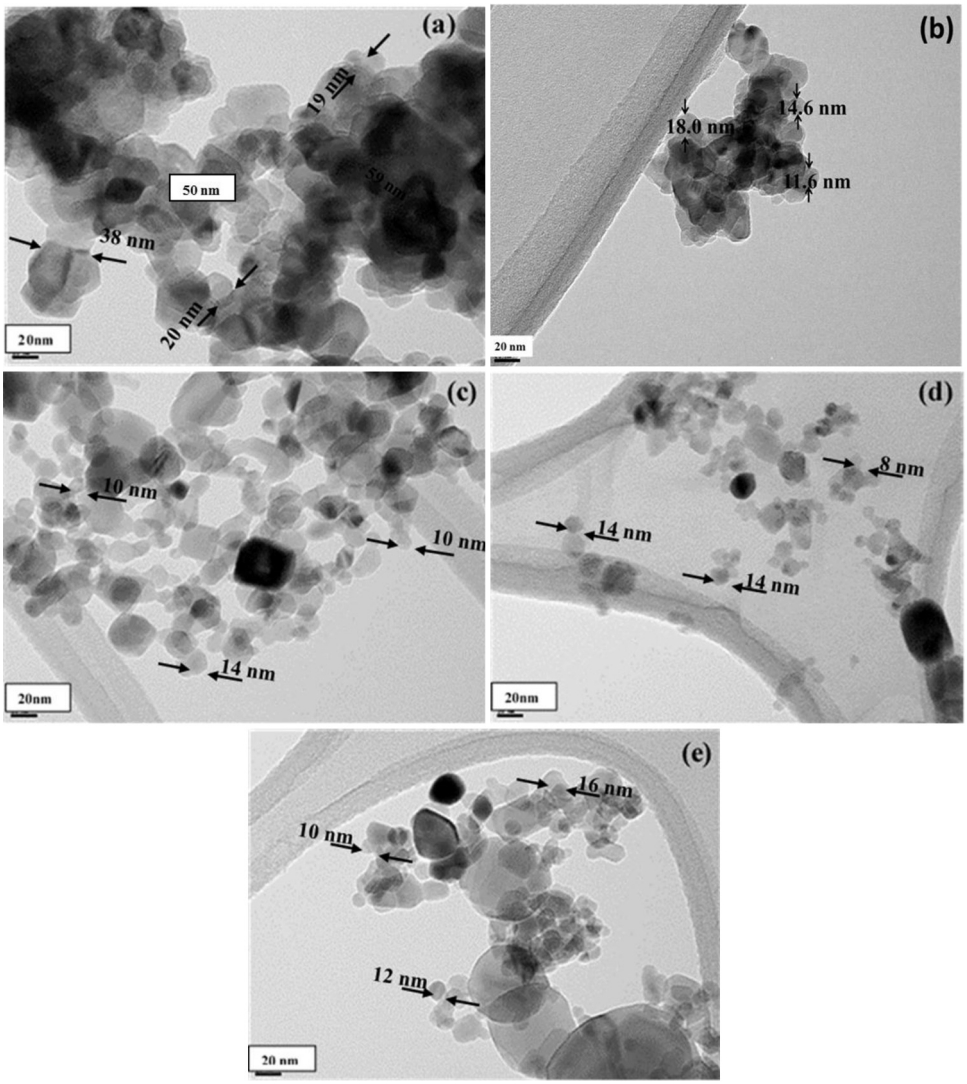

Fig. 4. TEM images of (a) co-precipitation Cr-TiO_2 catalysts, (b) sol–gel Cr-TiO_2 catalysts, (c) FSP Cr-TiO_2 catalysts, (d) R1 FSP Cr-TiO_2 catalysts and (e) RA1 FSP Cr-TiO_2 catalysts.

is around 70 for the fresh and R1, RA1 and R5 FSP Si/Ti/Cr catalyst and for RA5 FSP Si/Ti/Cr is 77 this increase in the phase is due the repeated calcination of the catalyst after the use. The thermal treatment has caused this increase in the anatase phase content for the FSP Si/Ti/Cr. The decrease in crystallite size indicates increase in structural defects that prevent grain growth. We did not observe any distinctive peaks for the Si in the FSP Si/Ti/Cr. These structural defects affect the crystallinity of the material and result in the reduction of the peak intensity and prevent the growth of the crystallite. This could be due the amorphous form of SiO_2. We have not detected any impurity diffraction peaks which indicate that most of the dopants have entered inside the TiO_2 lattice. However, fractions of chromium related impurity phases may be present on the surface or on grain boundary which may be beyond the detection limit of XRD.

3.3. UV–vis spectra

In Fig. 3(a) and (b), we have presented the FSP TiO_2 material along with the UV–vis absorbance spectra of the catalyst made by sol–gel, Co-precp, FSP Cr/TiO_2 and FSP Si/Ti/Cr for comparison. FSP TiO_2 is characterized by sharp absorption edges at about 391 nm (E_g–3.17 eV). The enhancement of the absorptions in the visible range from 400 to 650 nm with the Cr/TiO_2 catalyst made by sol–gel, Co-precp, FSP Cr/TiO_2 and FSP Si/Ti/Cr has accompanied with the changes on color from white to yellow [38]. The band gap is given in Table 2, shows the drop in the E_g from 3.17 eV for TiO_2 to 1.96 eV for sol–gel Cr/TiO_2, 1.73 eV for the co-precp Cr/TiO_2, 2.61 eV for FSP Cr/TiO_2 and 2.22 eV for FSP Si/Ti/Cr. The enhanced absorption observed for the Cr-TiO_2 samples in visible region can be considered to involve the excitation of the 3*d* electrons of the Cr ion to TiO_2 conduction band according to their respective energy levels [38,16–18]. The generation of new energy levels due to the injection of impurities into the TiO_2 lattice coupled with the generation of oxygen vacancies by Cr ion doping may contribute to the observed visible-light absorption of the Cr-TiO_2 samples. We have not observed significant changes in the absorption of the reused catalysts and reactivated catalysts.

3.4. Transmission electron microscopy (TEM)

Fig. 4a–e shows TEM images of sol–gel, Co-precp, FSP, R1 FSP and RA1 Cr/TiO_2 nanocrystals, respectively. In terms of particle shapes, the FSP-made Cr/TiO_2 nanocrystals consisting of irregular particles with round edges, whereas we can observe the round shape particles synthesized by the thermal synthesis (sol–gel and co-precp)

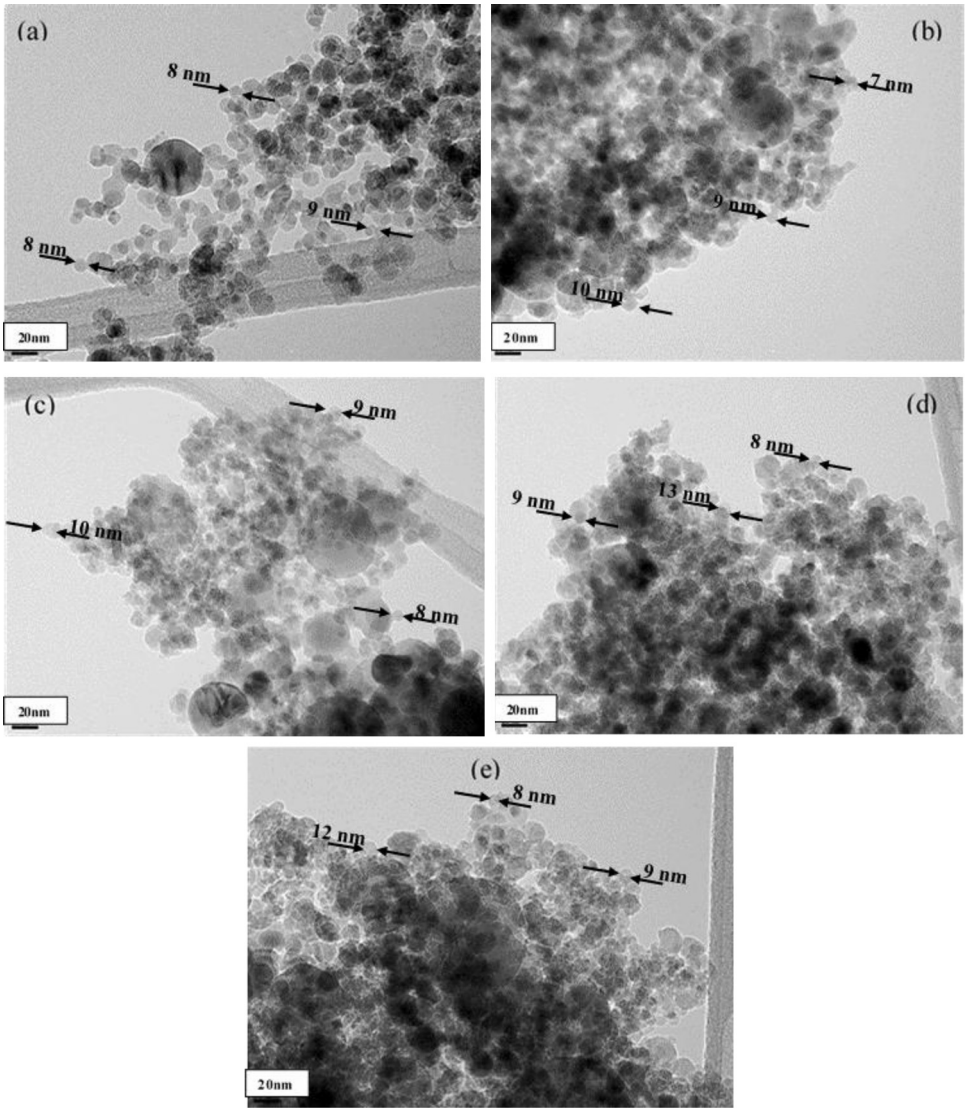

Fig. 5. TEM images of (a) FSP Si/Ti/Cr catalysts, (b) R1 FSP Si/Ti/Cr catalysts, (c) RA1 FSP Si/Ti/Cr catalysts, (d) R3 FSP Si/Ti/Cr catalysts and (e) RA3 FSP Si/Ti/Cr catalysts.

materials. The average particle size of Co-Precp Cr/TiO_2 is in agreement with the BET particle diameter, whereas the particle size of the sol–gel Cr/TiO_2 are larger than the diameter of the particles predicted from BET or XRD data. We can observe the agglomeration of the FSP Cr/TiO_2 in Fig. 4d and e where we observe the particle sizes are in agreement with the BET particle sizes. We can observe a slight increase in the particle sizes and for the R1 FSP Cr/TiO_2 but we can observe the formations of significantly larger particles for RA1 FSP Cr/TiO_2. This is caused due to the thermal treatment of the catalyst after the use. Formation of a new Cr phase could not be detected from XRD even at low Ti/Cr ratios, presumably due to the well dispersed and small segregated Cr grains.

Fig. 5a–e shows TEM images of pure, R1, R3, RA1 and RA3 FSP Si/Ti/Cr nanocrystals, respectively. The particle size of the samples is uniform and there is no significant change in the particle sizes of pure, reused and reactivated samples which is in agreement with the BET particle diameter. We can observe the agglomerations of the samples in Fig. 5a–e and the particle have more spherical outline when compared with FSP Cr/TiO_2 in Fig. 4c–e. We can observe the uniformity in the particle sizes provided by the addition of Si to the samples in Fig. 5a–e even for the samples which have gone through the thermal treatment for reactivation after the initial use. We did not find any separate phase made for SiO_2 which is also evident in our XRD runs.

3.5. Temperature-programmed reduction (H_2-TPR)

The TPR profiles of fresh, used and reactivated samples are shown in Fig. 6(a) and (b). As shown in Fig. 6(a), only one reduction peak appears at about 300 °C for the co-precp, R1 co-precp, sol–gel, and R1 sol–gel. The presence of only one reduction peak for the materials indicate the presence of single oxidation species (Cr(VI)). The same can be observed for FSP Cr/TiO_2 but the reduction temperature (258 °C) is lower than the above samples. There are two reduction peaks appearing at about 300 and 470 °C in the samples with R1 and RA1 FSP Cr/TiO_2, which proves that different oxidation states of Cr co-exist. This result is consistent with that of UV–vis spectra and the visual observation of the sample colors. The used catalyst has also shown the reduction in the activity of the catalyst even with the reactivation of the catalyst we have observed the presence of these two peaks. The peak at lower temperature corresponds to the Cr(IV) and the peak of the higher temperature is of Cr(III) which limits the activity of the catalyst. The reduction profiles of bulk CrO_3 comprise of the reduction peaks at 280, 462, and 585 °C. These peaks can be ascribed to the stepwise reduction

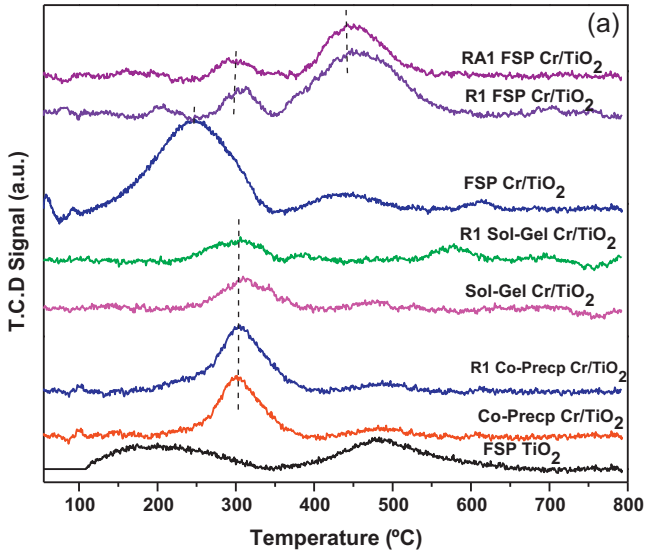

Fig. 6. H_2-TPR patterns of fresh, used reactivated catalysts made by (a) FSP TiO_2, FSP Cr/TiO_2, sol–gel and co-precipitation; (b) FSP Si/Ti/Cr (with atomic ratio of 20:20:2, reduction temperature range 50–800 °C).

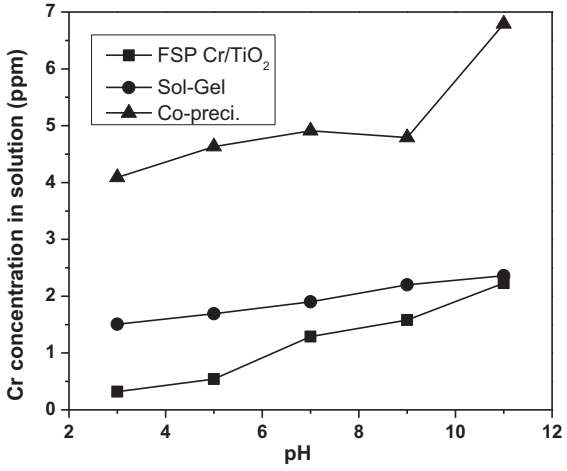

Fig. 7. Effect of pH on Cr leaching in Cr/TiO_2 FSP, $Cr\text{-}TiO_2$ sol–gel and $Cr\text{-}TiO_2$ co-precipitation catalysts (pH range 3–11).

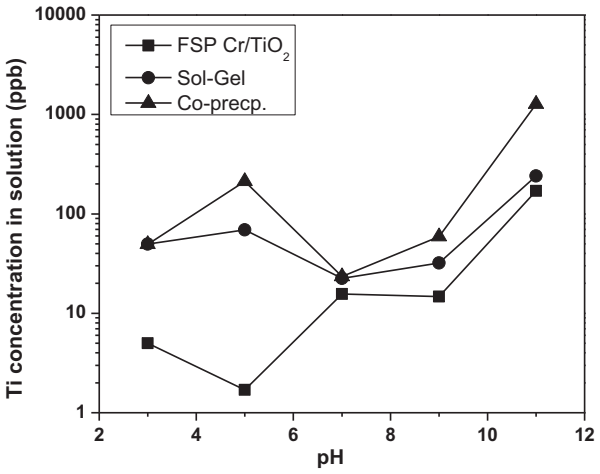

Fig. 8. Effect of pH on Ti leaching in Cr/TiO_2 FSP, $Cr\text{-}TiO_2$ sol–gel and $Cr\text{-}TiO_2$ co-precipitation catalysts (pH range 3–11).

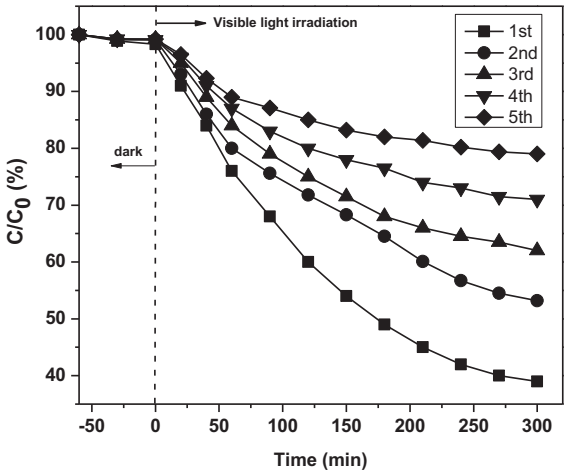

Fig. 9. Photocatalytic conversion with respect to time over FSP Cr/TiO_2 of 500 mL of 4-chlorophenol with 500 μm initial concentration and the effect of reused catalyst in visible light region.

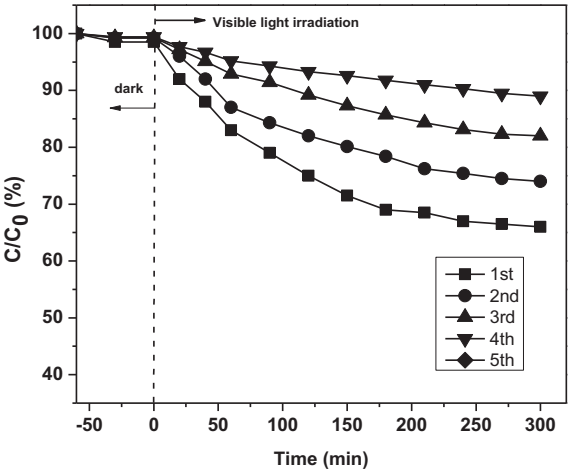

Fig. 10. Photocatalytic conversion with respect to time over sol–gel Cr/TiO_2 of 500 mL of 4-chlorophenol with 500 μm initial concentration and the effect of reused catalyst in visible light region.

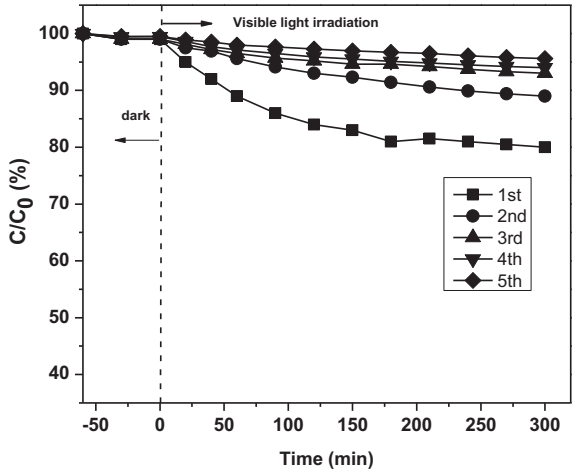

Fig. 11. Photocatalytic conversion with respect to time over co-precipitated Cr/TiO_2 of 500 mL of 4-chlorophenol with 500 μm initial concentration and the effect of reused catalyst in visible light region.

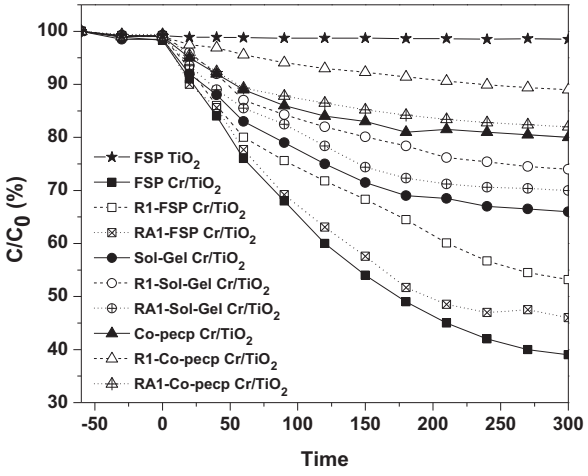

Fig. 12. The final photocatalytic conversion of FSP, sol–gel and co-precipitation $Cr-TiO_2$ catalyst with the effect of reused and reactivated catalyst in visible light region.

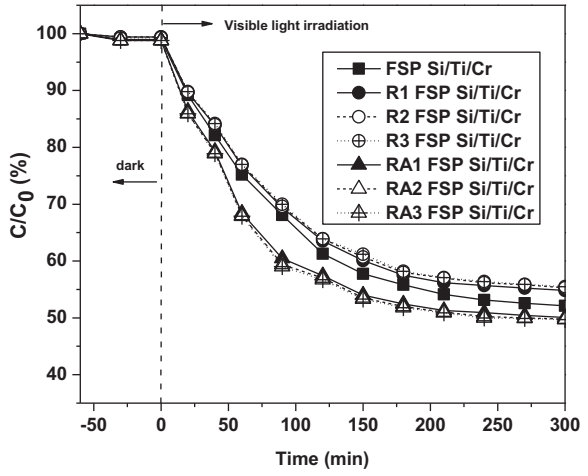

Fig. 13. Photocatalytic conversion with respect to time over FSP SI/Ti/Cr of 500 mL of 4-chlorophenol with 500 μm initial concentration and the effect of reused and reactivated catalyst in visible light region.

of $Cr^{6+} \rightarrow Cr^{5+}$, $Cr^{5+} \rightarrow Cr^{3+}$, and $Cr^{3+} \rightarrow$ either Cr^{2+} or the metallic state, respectively [16]. As shown in Fig. 6(a), FSP TiO_2 shows two peaks at 216 °C and 480 °C which can be ascribed to the partial reduction of TiO_2.

The TPR profile of FSP Si/Ti/Cr samples show two reduction peaks (Fig. 6(b)). The primary peak at 326 °C corresponds to the reduction of Cr^{6+} along with the effect of the interaction between Ti^{4+} and also with silica [39]. The reduction temperature of the peak is lower for R1 and RA1 FSP Si/Ti/Cr and increases for the R3 and RA3 FSP Si/Ti/Cr samples. We can observe the increase in the area of the first peak of the reactivated catalyst. The increase is caused due the thermal treatment of the catalyst. This is also evident for the sol–gel and Co-precp catalysts because the catalysts has gone through the thermal treatment in the synthesis process. The second peak at 474 °C corresponds to the reduction of bulk Cr(III). This peak is separated for the R1, RA1 and the separation can be clearly observed in the R3 and RA3 FSP Si/Ti/Cr catalysts.

3.6. Leaching studies by ICP-MS

While the use of the catalyst having metal ions, it has come to our attention that the metal leaching from the catalyst could cause a secondary contamination to wastewater in the environmental application. The various waste water streams in the environment may contain large range of the contaminations resulting in the extreme pH of the water. In the present work we have studied the broad pH range from 3 to 11. The concentration of Cr and Ti ions in the solution was measured by ICP after 24 h stirring at the given condition and the results are shown in Fig. 7 and Fig. 8, respectively. These concentrations in the solution directly reflect the extent of leaching from the catalyst during the reaction. In Fig. 7, we can see the effect of the synthesis methods on the leaching of the Cr. We can observe the increase in the Cr leaching as we increase the pH from 3 to 11 for all the samples. The Co-precp method has demonstrated higher leaching, namely 6.8 ppm for a pH of 11 and minimum of 4.1 ppm at pH of 3. The sol–gel method has lower leaching when compared with Co-precp and higher than FSP Cr/TiO_2. We have found the lower leaching in the FSP made catalyst. We have observed higher levels of leaching for FSP Cr/TiO_2 at pH of 11 (1.9 ppm). This level of Cr leaching suggested that among the given methods of synthesis even with the higher surface area the leaching is lower for the FSP made materials.

Unlike Cr leaching, Ti tends to leach out from the catalyst in a more irregular manner. We have observed a non-linear pattern with Ti concentration in the solution. We can observe that there is significantly lower amount of Ti (ppb levels) leaching when compared with Cr (ppm levels). Similar to Cr, here we also find that Co-precp. has more leaching of Ti followed by sol–gel and FSP methods. This indicates that there is a significant amount of secondary contamination while application of the photocatalytic degradation of the organic pollutant in the waste water stream. These results also indicate that the FSP made samples results in stronger bonding between Ti and Cr in than the catalysts made by sol–gel and Co-precp. methods. The lowest concentration in solution was about 0.25 mg/L for the lowest pH of 3 used for the FSP made catalysts. This concentration is well beyond the threshold permitted value for Cr(VI) which is about 0.05 mg/L. For this reason, we should be careful in regarding the use of Cr containing catalysts for practical water treatment [40].

3.7. Photocatalytic performance of catalysts in visible region

In the present work, we operated the reactor in semi-batch mode where 500 mL of 500 μm 4-chlorophenol in aqueous solution is kept in the reactor vessel with 400 mg of the catalyst with

air flow of 500 cc/min. For the photocatalytic testing of the catalysts specified, several modifications of the conventional reactor setup were necessary. More specifically, one needs to assure that only visible light reaches the catalyst suspension. We have used the double layer acrylic OP-2 (Museum quality) sheet was placed between the light source and the reactor to ensure that only visible light reaches the reactor. Here, the independent variables are the inlet concentration (C_{A0}) and time. The dependent variable is the fractional conversion. The photocatalytic oxidation of 4-chlorophenol in the present study was followed by measuring the TOC concentration. The overall mineralization process was traced by measuring the total carbon (TC) concentration in solution.

The curves of 4-chlorophenol concentration are by different samples are shown in Figs. 9–13 for the various sample. On the basis of the surface characterization results described above, it is now instructive to compare the photocatalytic activities of all as-prepared catalyst materials. Fig. 9 shows the visible photocatalytic degradation of 4-chlorophenol in the visible region in the presence of the FSP Cr/TiO_2. The conversion of the 4-chlorophenol after 5 h for the fresh catalyst was 61% which is higher than the used catalyst. We can observe the reduction in the catalyst activity of the used materials as they go through the cycles R1–R4. Similar observation was found for the catalyst synthesized by the sol–gel method and the co-precp methods in the Fig. 10 and Fig. 11, respectively.

In Fig. 12, we can observe the final conversions of the catalyst synthesized by sol–gel, co-precp and FSP Cr/TiO_2. We can clearly observe the reduction in the catalyst activity for all the materials. The fresh catalyst made by FSP Cr/TiO_2 has superior activity for the first cycle which is due to the higher surface area and the presence of Cr(IV). There is good correlation between the photocatalytic activity, surface area and the presence of Cr(IV). The reduction in the photocatalytic activity of the catalyst also corresponds to the formation of agglomerates of the samples along with reduction of the Cr(IV) as suggested by the TPR results. This decrease in the activity of the catalyst could have also been the direct result of leaching of the Cr ion in the liquid stream thus reducing the number of Cr ions available on the surface of the catalyst. Therefore, we conclude that the catalytic activity depends on the catalysts preparation method and the structure of the support material. From the TPR studies one can clearly observe that the presence of hexavalent chromium is significantly higher than trivalent species adds to the activity of the catalyst [37–42].

One of the principal causes for the reduction of the activity is the reduction of Cr(IV) in the samples during the photocatalysis process. To overcome this challenge we tried to reactivate the used catalyst by thermal treatment [12]. In Fig. 12 we can observe the enhancement of the photocatalytic activity of the reactivated catalyst when compared with reused catalyst. There is significant improvement in the photocatalytic activity of the reactivated catalyst which is due to the increase of the Cr(IV) as given by our TPR experiments. In spite of the improvement in the photocatalytic activity of the reactivated catalyst there is decrease in the activity of RA1 when compared with the fresh catalyst. This is due to the reduction in the BET surface area of the catalyst due to the heat treatment.

To overcome the above challenge and to stabilize the structure of the materials we have taken the best syntheses method FSP and incorporated Si to the catalyst to enhance the structural stability [13,22–23]. The synthesized FSP Si/Ti/Cr material was tested for the stability with and without reactivation of the used sample. Fig. 13 show the photocatalytic degradation of the 4-cholorophenol with the FSP Si/Ti/Cr and the effect of reuse of the catalyst with and without reactivation of the used materials. In Fig. 13 we can observe the stability of the material and the activity of the catalyst was stable for the 3 runs. The R1–R3 samples have similar activity which is attributed to the stability and constant surface BET surface area of the materials after the three uses. A similar observation was found for the RA1–RA3 catalyst but the activity of the reactivated materials is higher than fresh and used catalyst. This enhancement of the activity by the reactivated catalyst is in agreement with the Cr(IV) concentration given by our TPR data. We found the higher Cr(IV) concentration in the reactivated materials which is a significant factor for the improvement in the photocatalytic activity of the materials. We have observed the improvement in the activity with the addition of Si as a support and it also caused the improvement in the surface area and structural stability.

4. Conclusions

We have observed that the flame spray pyrolysis (FSP) Cr-TiO_2 has superior activity when compared with the other given synthesis methods (sol–gel and co-precipitation). There was only anatase phase present for the sol–gel and co-precipitation made materials. The FSP made catalyst has surface area of 57 m^2/gr which is higher than the other catalyst (17 m^2/gr and 36.5 m^2/gr for sol–gel and co-precipitation, respectively). TPR results indicated the higher presence of the Cr^{+6} for the FSP made catalyst which had significant influence in the activity of the catalyst. All the catalysts tested showed the reduction in their activity which was a result of reducing the Cr^{+6} species of the catalyst along with the agglomeration. The leaching of the Cr into the liquid phase for pH (3–11) was studied of the FSP made catalyst was found to be minimal with respect to other synthesis methods. For this reason there should be careful consideration for use of Cr containing catalysts for practical water treatment. Si/Ti/Cr catalyst was developed by FSP method which endures and stabilizes the photocatalytic activity of the catalyst. The BET surface area of the FSP Si/Ti/Cr catalyst was stable even with the reactivated catalyst. The developed catalyst also demonstrated the advantage of low metal leaching during the catalytic reaction, thus avoiding secondary metal contamination to the treated wastewater. We found that the higher Cr(IV) concentration in the reactivated materials which is a significant factor for the improving in the photocatalytic activity of the materials. We have observed the enhancement in the activity with the addition of Si as a support and it also caused the improvement in the surface area and structural stability.

Acknowledgements

The authors wish to acknowledge EPA/Pegasus contract (contract number EP-C-11-006) for financial support of this work through the scholarship to Siva Nagi Reddy Inturi.

References

[1] A. Fujishima, K. Honda, Nature 238 (1972) 37–38.
[2] J. Peral, X. Domenech, D.F. Ollis, J. Chem. Technol. Biol. 70 (1978) 117.
[3] M.R. Hoffmann, S.T. Martin, W.Y. Choi, D.W. Bahnemann, Chem. Rev. 95 (1995) 69–96.
[4] A.L. Linsebigler, G. Lu, J.T. Yates Jr., Chem. Rev. 95 (1995) 735–758.
[5] R.W. Matthews, Water Res. 24 (1990) 653.
[6] M.A. Fox, M.T. Dulay, Chem. Rev. 93 (1993) 341–357.
[7] M. Anpo, M. Takeuchi, J. Catal. 216 (2003) 505–516.
[8] R. Asahi, T. Morikawa, T. Ohwaki, K. Aoki, Y. Taga, Science 293 (2001) 269–271.
[9] Y.M. Xu, C.H. Langford, J. Phys. Chem. 99 (1995) 11501–11507.
[10] J.C. Yu, G.S. Li, X.C. Wang, X.L. Hu, C.W. Leung, Z.D. Zhang, Chem. Commun. (2006) 2717.
[11] L. Davydov, E.P. Reddy, P. France, P.G. Smirniotis, J. Catal. 203 (2001) 157–167.
[12] E.P. Reddy, B. Sun, P.G. Smirniotis, J. Phys. Chem. B 108 (2004) 17198–17205.
[13] S.V. Awate, N.E. Jacob, S.S. Deshpande, T.R. Gaydhankar, A.A. Belhekar, J. Mol. Catal. A 226 (2005) 149–154.
[14] V.R. Elias, E.G. Vaschetto, K. Sapag, M.E. Crivello, S.G. Casuscelli, G.A. Eimer, Top. Catal. 54 (2011) 277–286.
[15] F.C. Marques, M.C. Canela, A.M. Stumbo, Catal. Today 133 (2008) 594–599.
[16] B. Sun, E.P. Reddy, P.G. Smirniotis, Appl. Catal. B: Environ. 57 (2005) 139–149.
[17] S.N.R. Inturi, T. Boningari, M. Suidan, P.G. Smirniotis, Appl. Catal. B: Environ. 144 (2014) 333–342.

[18] S.N.R. Inturi, T. Boningari, M. Suidan, P.G. Smirniotis, J. Phys Chem. B 118 (2014) 231–242.
[19] Y.M. Sung, J.S. Park, T.G. Kim, J. Nano-Cryst Solids 358 (2012) 182–187.
[20] T. Ivanova, A. Harizanova, T. Koutzarova, B. Vertruyen, Opt. Mater. 36 (2013) 207–213.
[21] J.M. Du, H.J. Chen, H. Yang, R.R. Sang, Y.T. Qian, Y.X. Li, G.G. Zhu, Y.J. Mao, W. He, D.J. Kang, Micropor. Mesopor. Mater. 182 (2013) 87–94.
[22] G.K. Zhang, X. Sheng, Y.Q. Yang, J. Phys. Chem. C 115 (2011) 7145–7152.
[23] A. Moiseev, F. Qi, J. Deubener, A. Weber, Chem. Eng. J. 170 (2011) 308–315.
[24] P. Wang, J. Wang, X.F. Wang, H.G. Yu, J.G. Yu, M. Lei, Y.G. Wang, Appl. Catal. B: Environ. 132–133 (2013) 452–459.
[25] P. Gao, D.D. Sun, Appl. Catal. B: Environ. 147 (2014) 888–896.
[26] L. Madler, KONA 22 (2004) 107–120.
[27] R. Strobel, A. Baiker, S.E. Pratsinis, Adv. Powder Technol. 17 (2006) 457.
[28] S.E. Pratsinis, Prog. Energ. Combust. 24 (1998) 197–219.
[29] L. Madler, H.K. Kammler, R. Mueller, S.E. Pratsinis, Aerosol Sci. 33 (2002) 369–389.
[30] W.Y. Teoh, L. Madler, D. Beydoun, S.E. Pratsinis, R. Amal, Chem. Eng. Sci. 60 (2005) 5852–5861.
[31] Y.C. Chen, A.V. Vorontsov, P.G. Smirniotis, Photochem. Photobiol. Sci. 2 (2003) 694–698.
[32] S. Brunauer, L.S. Deming, W.E. Deming, E. Teller, J. Am. Chem. Soc. 62 (1940) 1723–1732.
[33] J. Falong, H. Yan, T. Yiwen, Z. Lizhi, Powder Technol. 176 (2007) 130–136.
[34] L. Jinyou, S. Yanwei, D. Bin, Y. Jianmao, Y. Jianyong, S.A. Salem, Marine Pollut. Bull. 64 (2012) 347–352.
[35] R. Jenkins, R.L. Snyder, (1996) Introduction to X-ray Powder Diffractometry; Wiley & Sons, Inc.
[36] C. Biswajit, C. Amarjyoti, Mater. Sci. Eng. B 178 (2013) 794–800.
[37] H. Schulz, L. Mädler, R. Strobel, R. Jossen, S.E. Pratsinis, J. Mater. Res. 20 (2005) 2568–2577.
[38] B. Sun, E.P. Reddy, P.G. Smirniotis, Sci. Technol. 39 (2005) 6251–6259.
[39] B. Sun, E.P. Reddy, P.G. Smirniotis, J. Catal. 237 (2006) 314–321.
[40] D.E. Tsydenov, A.A. Shutilov, G.A. Zenkovets, A.V. Vorontsov, Chem. Eng. J 251 (2014) 131–137.
[41] J.M. Herrmann, J. Photochem. Photobiol. A 216 (2010) 85–93.
[42] L. Zang, C. Lange, I. Abraham, S. Storck, W. Maier, H. Kisch, J. Phys. Chem. B 102 (1998) 10765–10771.